Available online at www.sciencedirect.com
ScienceDirect
Journal of the European Ceramic Society 31 (2011) 2481–2487
www.elsevier.com/locate/jeurceramsoc

Electron-energy loss spectroscopy and Raman studies of nanosized chromium carbide synthesized during carbothermal reduction process from precursor $Cr(CO)_6$

Hao-Tung Lin [a], Pramoda K. Nayak [b], Sheng-Chang Wang [c], Shin-Yun Chang [b], Jow-Lay Huang [b,*]

[a] *Electrical Technology Center, Cheng Shiu University, Kaohsiung County 833, Taiwan*
[b] *Department of Materials Science and Engineering, National Cheng-Kung University, Tainan 701, Taiwan*
[c] *Department of Mechanical Engineering, Southern Taiwan University, Tainan County 710, Taiwan*

Available online 3 January 2011

Abstract

Nanosized chromium carbide has been prepared by metal–organic chemical vapour deposition (MOCVD) method in a fluidized bed and carburized in the mixture of CH_4/H_2 atmosphere in temperature range 700–850 °C. The carburization process involves carbon deposition on the outer surface of the Cr_2O_3 powder, followed by carbon diffusion into the powder, leading to formation of metastable Cr_3C_{2-x} phase and stable Cr_3C_2. The phase transformation from Cr_2O_3 to Cr_3C_2 via an intermediate state Cr_3C_{2-x} has been identified using electron-energy loss spectroscopy (EELS) and micro-Raman spectroscopy. We could hypothesize that the formation of carbon nanofilms surrounding the carbide crystallites provides the stress and assist the phase transformation from metastable Cr_3C_{2-x} to stable Cr_3C_2.

Keywords: Precursors-organic; Nanocomposites; Spectroscopy; Al_2O_3; Carbides

1. Introduction

Over the past several decades, there have been efforts on improving the strength and the toughness of alumina, by the use of nanocomposites.[1–4] The incorporation of hard particulate reinforcement has been shown to be an easy, safe and economically toughening technique for alumina ceramics. The carbides are good reinforced materials for oxide ceramics due to their high melting point, high hardness, high Young modulus and wear resistance. Among the carbides, the Cr_3C_2 used for the second phase has been proved to exhibit improved mechanical properties and enhanced temperature oxidation resistance of Cr_3C_2/alumina composites.[3–5] In addition, Cr_3C_2 is a material with high electrical conductivity and the Cr_3C_2/ceramic composite has potential applications for electrical discharge machining (EDM).[6]

The mostly reported Cr_3C_2 were prepared from the reduction of chromium oxide by methane gas.[7] However, besides the three stable chromium carbides such as Cr_3C_2, Cr_7C_3, and $Cr_{23}C_6$, several metastable carbides were reported including Cr_3C, CrC_{1-y}, Cr_5C_2, and Cr_3C_{2-x} which were exist during different preparation methods and for various Cr/C contents.[8–10] Lerch and Rousset[11] indicated that the $CrO_{1.9}$ with high surface area (200–350 m^2/g) reduces at 700 °C in the mixture of methane and hydrogen atmosphere and produces Cr_3C_2 and metastable Cr_3C_{2-x}. The metastable Cr_3C_{2-x} powder was also prepared by Loubière et al.[12,13] using CH_4–H_2 atmosphere to carburize metastable chromium oxide. Summarizing above literatures, it is observed that the metastable Cr_3C_{2-x} is a Re_3B-type structure which can be found by carburization of high specific surface chromium oxide and usually present together with Cr_2O_3, Cr_3C_2 and free carbon.

Electron energy loss spectroscopy gives information about the electronic structure of chromium and carbon in Cr_3C_2. Lozzi et al.[14] have studied the electronic structure of Cr clusters on graphite by measuring $L_{2,3}$ ionization edges using EELS technique. They observed that there is a variation in the intensity ratio of L_3–L_2 ionization core edges. The EELS core edge energy is that required to excite an electron from a core level to the first unoccupied state above Fermi level E_f. Therefore, these variations in L_3/L_2 ratio are due to the empty d states above E_f. Fan et al.[15] have studied the electronic structure of Cr as well

* Corresponding author. Tel.: +886 6 2348188; fax: +886 6 2763586.
E-mail address: JLH888@mail.ncku.edu.tw (J.-L. Huang).

0955-2219/$ – see front matter © 2010 Elsevier Ltd. All rights reserved.
doi:10.1016/j.jeurceramsoc.2010.12.005

as carbon of chromium-doped diamond like-carbon films from Carbon K edge and Cr L edge using EELS analysis.

Raman spectroscopy is a best tool for characterization of carbon based materials. Different Raman modes for diamond, graphite and amorphous carbon have been studied by different groups.[16–18] Barshilia et al.[19] have studied the Raman spectra of Cr_xO_y/Cr/Cr_2O_3 multilayer coatings on Cu substrates. They have observed the A_{1g} and E_g Raman modes, which are the characteristic of Cr_2O_3.

In our previous study,[20,21] Cr_2O_3/Al_2O_3 composite powders were prepared by the decomposition of chromium hexacarbonyl in a fluidized bed. The composite powder then hot-press sintered in a graphite mode and transformed as Cr_3C_2/Al_2O_3 nanocomposite. But some residual Cr_2O_3 reacted with Al_2O_3 in high temperature became solid solution thereby decreasing Cr_3C_2 contents. In order to carburize the chromium oxide completely, the present paper reports the nanosized chromium carbide from precursor carburization in a CH_4/H_2 mixture gas. The phase evolution and formation mechanisms were characterized by the EELS and micro-Raman spectroscopy.

2. Experimental procedure

The decomposed powder was fabricated by metal–organic chemical vapor deposition (MOCVD) method in a fluidized bed. The schematic diagram of the homemade apparatus is given in our earlier paper.[22] The precursor comprising of metal–organic chromium hexacarbonyl ($Cr(CO)_6$, 99% Strem Chemicals Co., USA) was initially heated for evaporation at 75 °C. He gas was used as the carrier gas for transporting these precursor vapors into the reaction chamber for coating on the fluidized alumina powder (α-Al_2O_3, 99.9%, A16SG, Alcoa, USA), which was used as the matrix powder. The pressure of reaction chamber was controlled at 10 torr and the reaction temperature was kept at 300 °C. The as-received powder then carburized in an alumina tube furnace in the presence of methane–hydrogen mixture (1: 9) gas at 700–850 °C for 5 h.

The electron-energy loss spectroscopy (EELS) of prepared samples was characterized by field emission gun scanning transmission electron microscopy (FEG-STEM) equipped with energy dispersive X-ray detector (EDS) and energy filter (Gatan). The presence of the chromium oxide, carbide and carbon phases was analyzed by micro-Raman spectroscopy using a solid laser (514.5 nm) with an output power of 50 mW for 30 seconds (LabRAM HR). The Raman spectra are taken in the range of 1100–1800 cm^{-1} and 200–800 cm^{-1} for the detection of C–C and Cr binding energy, respectively. The microstructures have been studied by (FE-SEM, PHILIPS / FEI XL 40) and (FEG-TEM, TEI Tecnal F20, USA).

3. Results and discussion

The pyrolysis of Cr based precursor $Cr(CO)_6$ at 300 °C results the formation of Cr_2O_3, C–Cr and C–C bonds observed from XPS spectra.[22] The decomposed precursor deposits uniformly over Al_2O_3 and the deposited nanoparticles (∼30 nm) are shown in the TEM micrograph (Fig. 1(a)). The insert shows the TEM pattern of the deposited nanoparticles, which is amorphous in nature. From the EDS spectrum shown in Fig. 1(b), it is confirmed that the nanoparticles consist of mostly Cr and O along with small amount of C. The presence of Cu is the contribution from Cu grid.

Fig. 2 shows the EELS spectra of Cr L edge for the sample of the decomposed precursor and the samples carbonized at 800 °C and 850 °C. The chromium L edges have features comprising two sharp L_2 and L_3, known as "white lines"[14] and a continuum background following the edge. The sharp double peaks are due to transitions from the $2p^{1/2}$ and $2p^{3/2}$ core levels towards 3d states above E_f. The sharp peaks of L_2 and L_3 at threshold are due to the transitions from the $2p^{l/2}$ core levels to $3d^{3/2}$ states and the $2p^{3/2}$ core levels to $3d^{3/2}$ $3d^{5/2}$, respectively. The L_3/L_2 white line ratio is correlated to the electron occupancy and spin pairing in 3d band. The variations of the ratio are due to the interaction between chromium and surrounding atoms. A change of the L_2, L_3 edge intensities in the samples indicates a variation of the d holes because the edge intensity is proportional to the number of the empty final states available. The ratio of L_3/L_2 of sample shown in Fig. 2(a) is higher than that of carbonized samples. According to the results of Arévalo-López et al.[23] the ratio of L_3/L_2 for the Cr_2O_3 is about 1.6 and from the report of Fan et al.[15] the ratio of L_3/L_2 for the Chromium carbide is about 1. A comparison between Fig. 2(b) and (c) shows L_3 edge of the sample carbonized at 850 °C is 577.72 eV, while that of sample carbonized at 800 °C is 575.42 eV. The shift in energy (2.3 eV) is called the chemical shift. This result is due to the transformation from the metastable carbide to stable carbide, because the EELS represent the difference in energy between a core-level initial state and the lowest energy final state of an excited electron. But the energy loss close to 577.72 eV for the decomposed precursor,[24] which consists of Cr_2O_3 is same as the sample carbonized at 850 °C. It is observed that there is no chemical shift between this two species because Cr_2O_3 and Cr_3C_2 are both chemically stable compounds.

The π electron formed sp^2 bonding observed from the EELS spectra of C K edges as shown in Fig. 3. The peak of sp^2 bonding is sharper when the carbonized temperature increases from 800 °C to 850 °C. The sharpening of sp^2 peak is attributed to the formation of graphite like carbon according to Fan et al.[15] In Cr_3C_2, C is graphite like rather than diamond like, which comprising of sp^3 bonded carbon atoms. For the as decomposed precursor, the content of carbon was little and formed amorphous phase. More carbon produced from the pyrolysis of methane coated on the Cr_2O_3 surface and then formed graphite phase and metastable carbide of Cr_3C_{2-x}, when the sample was treated at 800 °C for 5 h. The increase of treated temperature to 850 °C, enhanced the process of carbonizing reaction leading to more graphite formation followed by transformation of metastable Cr_3C_{2-x} to stable carbide of Cr_3C_2.

The SEM micrographs of the decomposed precursor at different carburized temperature are shown in Fig. 4. The as decomposed precursor exhibits particle size of 20–30 nm shown in Fig. 4 (a) and the particle size increases with the increase of carburized temperature observed from Fig. 4(b)–(e). The maxi-

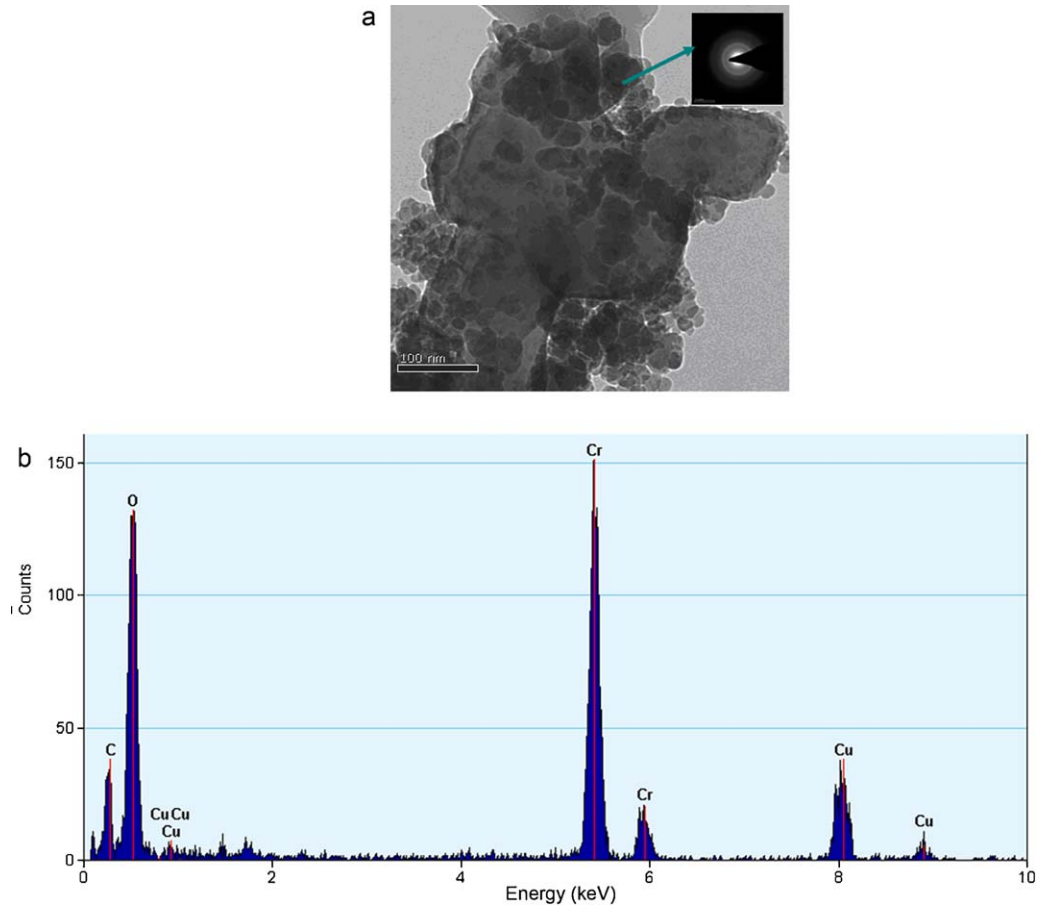

Fig. 1. TEM micrographs of (a) nanoparticles deposited on alumina particle and (b) EDS spectrum of the coating particle.

mum particle size is observed to be 150–200 nm for the precursor carburized at 850 °C for 5 h. Similar trend in particle size has also been observed from the TEM morphology of the decomposed powder at different carburized temperature (Fig. 5). From TEM microstructures, it is observed that the carbon layers are coated on Cr_2O_3 surface and the coating is very effective at higher temperatures in the range 800–850 °C.

The presence of the chromium oxide, carbide and carbon phases of the decomposed powder at different temperature has been analyzed by micro-Raman spectroscopy as shown in Fig. 6.

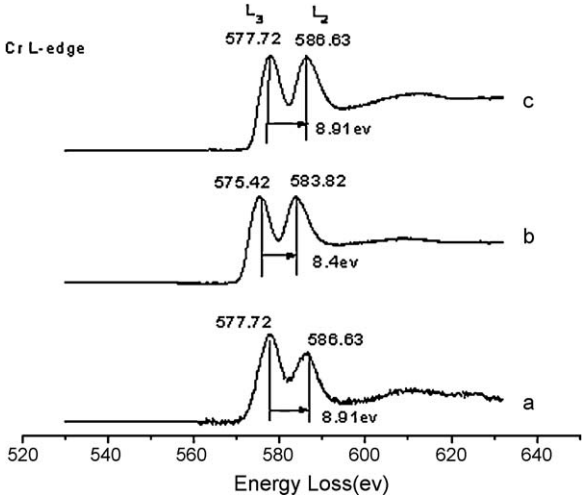

Fig. 2. EELS of Cr L edges: (a) decomposed precursor, (b) carbonized at 800 °C/5 h (Cr_3C_{2-x}), and (c) carbonized at 850 °C/5 h (Cr_3C_2).

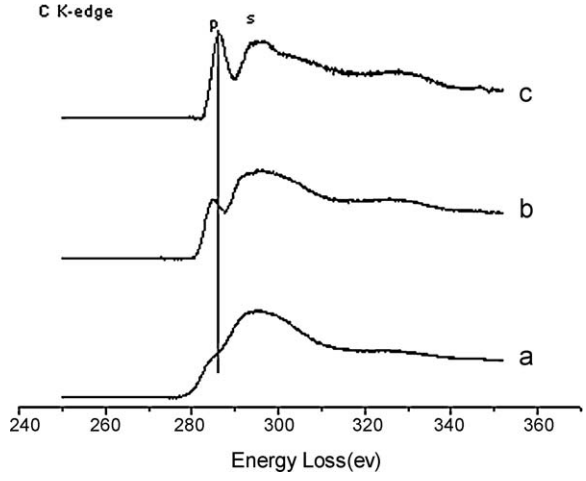

Fig. 3. EELS of C K edges: (a) decomposed precursor, (b) carbonized at 800 °C/5 h (Cr_3C_{2-x}), and (c) carbonized at 850 °C/5 h (Cr_3C_2).

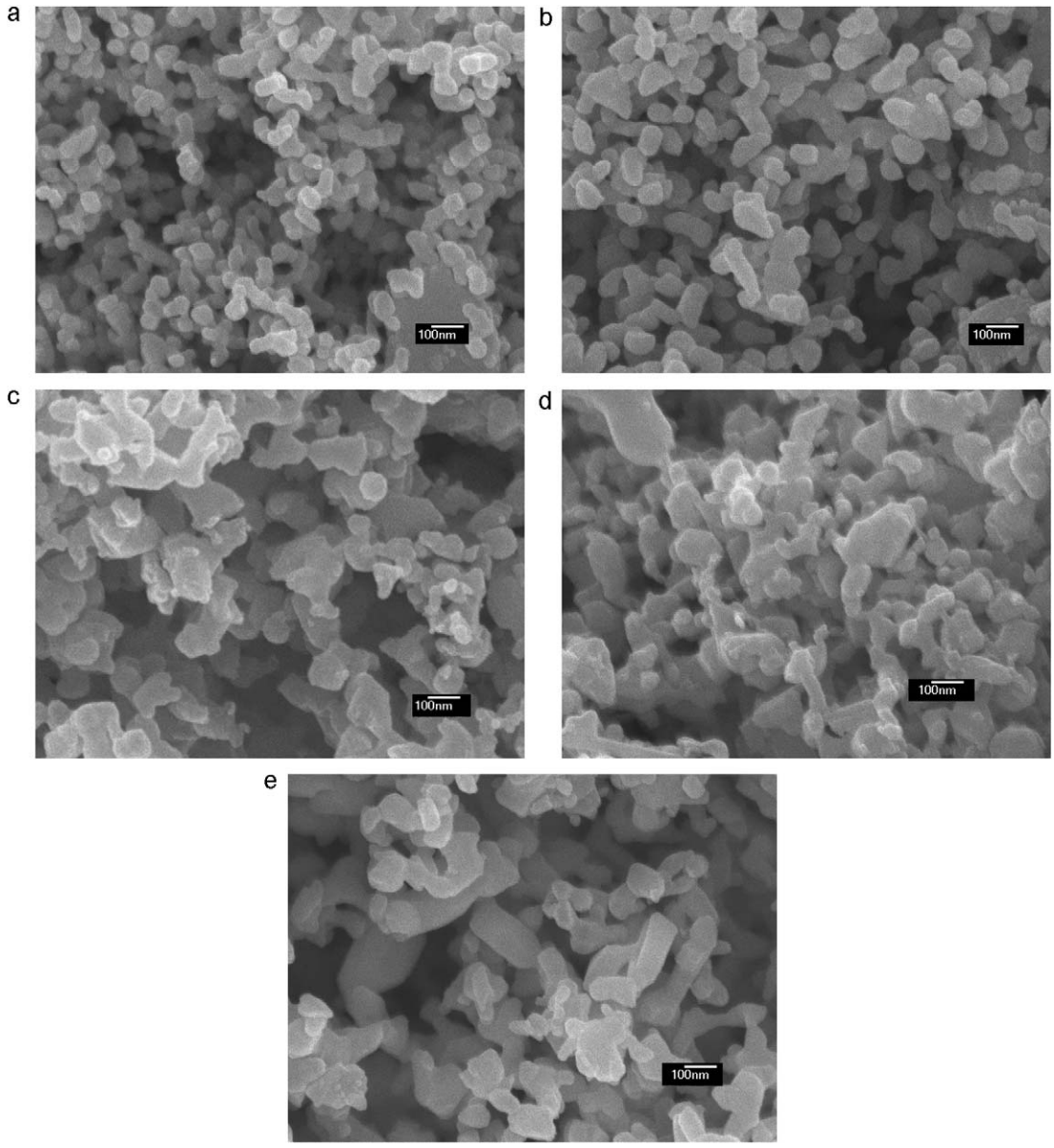

Fig. 4. SEM micrographs of decomposed precursor: (a) as prepared, and carburized at (b) 700 °C, (c) 750 °C, (d) 800 °C, and (e) 850 °C for 5 h.

The feature of the powder of as decomposed precursor is not obvious, i.e. the content of free carbon bonds is very little. After carbonized treatment increases from 700 °C to 850 °C, the peak of D-bands and G bands become more prominent. The D-band is called as the disorder or defect band and the G-band corresponds to the graphite band, i.e. sp^2 bonded carbon atoms. The Intensity of G band peaks increases with higher carbonization temperatures means there is presence of more graphite and carbide. Moreover, increased I_D/I_G ratio indicates an increase in the sp^2 bonding according to Lacerda et al.[25] It is consistent with the results of TEM images showing the carbon layers coating on the Cr_2O_3 surface. The Raman spectra of the decomposed powder at different temperature taken in the range of 200–800 cm^{-1} are shown in Fig. 7. The peaks at 542 cm^{-1} and (302, 341, 596 cm^{-1}) corresponds to Raman A_{1g} and E_g modes of Cr_2O_3.[19] The intensities of Cr_2O_3 at these peak positions are comparable between 700 °C and 750 °C, while these are reduced slightly at 800 °C and 850 °C. This gives information about the transformation trend from Cr_2O_3 to Cr_3C_2 but not completely conversion.

Based on these above results, we could hypothesize the following phase transformation steps: In the first step, the methane decomposes to elemental carbon and hydrogen.[26,27] The carbon reacts with the Cr_2O_3 at temperatures higher than 800 °C, and produce partial Cr_3C_2 phase and $CO_{(g)}$. The $CO_{(g)}$ can also carburize the Cr_2O_3 further. There are three kinds of carbon sources in the system viz. free carbon from the decomposition of methane, CO from above reaction and C–C bonding from

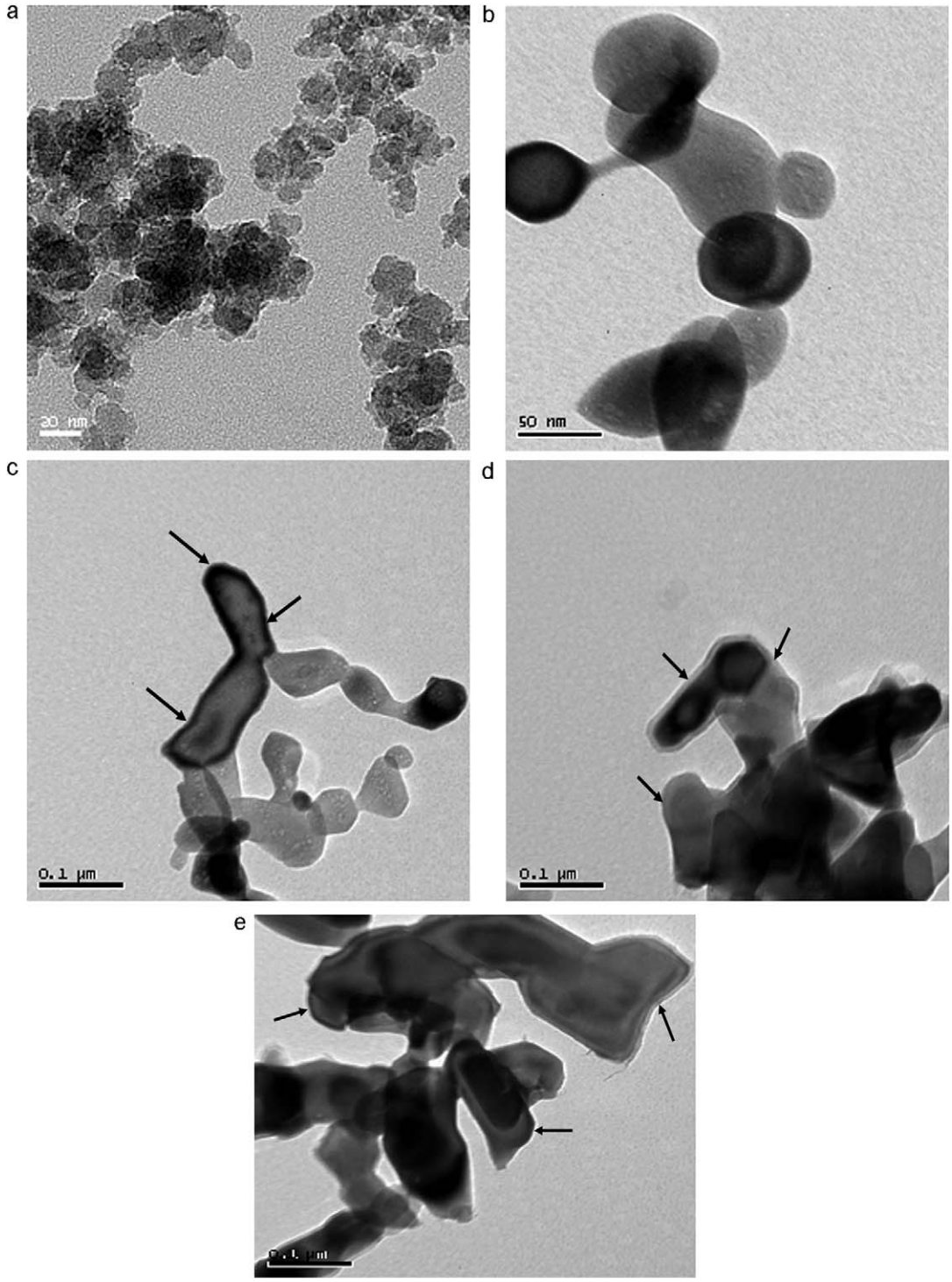

Fig. 5. TEM morphology of decomposed precursor: (a) as prepared, and carburized at (b) 700 °C, (c) 750 °C, (d) 800 °C, and (e) 850 ° C for 5 h. The carbon layers on Cr_2O_3 particles are marked by arrows.

the precursor. Finally, the unreacted redundant carbon sources would deposit on the surface of the powder as the lamellar graphene. The graphene deposited during the carburization has an important role for the formation of meta-stable Cr_3C_{2-x} and stable Cr_3C_2. Initially, carbon gets absorb on the surface of chromium oxide at low temperature. As the temperature rises, substantial amount of carbon is available, leading to metastable chromium carbide. Finally, as the temperature increases further, the redundant carbon forms the graphene layers. Further thickening of the graphene films, generates a mechanical stress[13] which assists the transformation of meta-stable Cr_3C_{2-x} state to stable Cr_3C_2 phase.

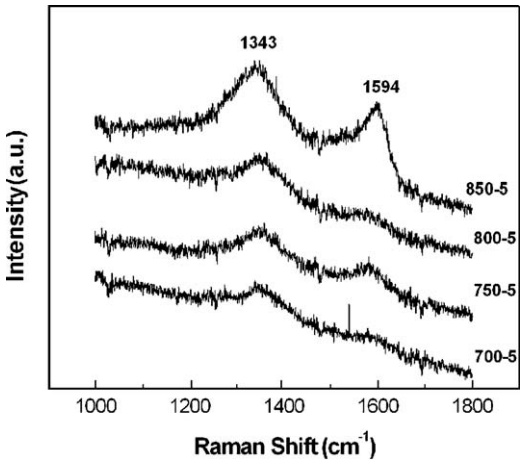

Fig. 6. Raman spectra of decomposed powder at different temperature in the range of 1100–1800 cm^{-1}.

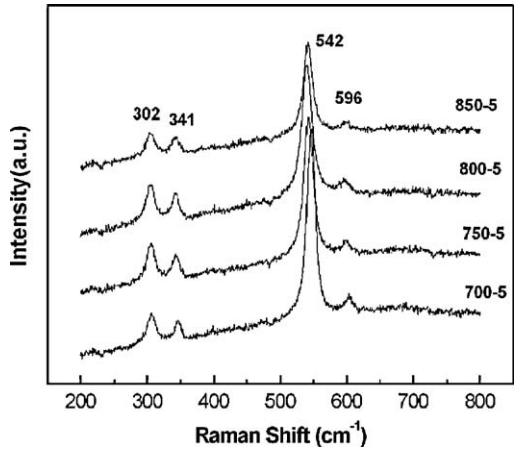

Fig. 7. Raman spectra of decomposed powder at different temperature in the range of 200–800 cm^{-1}.

4. Conclusion

The $Cr(CO)_6$ powder is decomposed by MOCVD fluidized bed and form an amorphous Cr_2O_3 with free C–C bonding and C–O bonding through the carbonized treatment under the CH_4–H_2 atmosphere. Electron-energy loss spectroscopy and micro-Raman analysis reveal that the decomposed powder transforms from chromium oxide to chromium carbide [Cr_2O_3 (700 °C) → Cr_3C_{2-x} (800 °C) → Cr_3C_2 (850 °C)] via an intermediate metastable state. Initially, the decomposed carbon from methane adsorbs on the surface of chromium oxide. With the increase of temperature, the chromium oxide transforms to chromium carbide.

Acknowledgments

Authors are thankful to National Science Council of Taiwan for its financial support under the contract No: 99-2923-E-006-002-MY3.

References

1. Niihara K. New design concept of structural ceramics–ceramic nanocomposite. *J Ceram Soc Jpn* 1991;**99**(10):974–82.
2. Nawa M, Sekino T, Niihara K. Microstructure and mechanical properties of Al_2O_3–Mo nanocomposites. *J Jpn Soc Powder Powder Metall* 1992;**39**:1104–8.
3. Nakahira A, Niihara K. Sintering behaviors and consolidation process for Al_2O_3/SiC nanocomposites. *J Ceram Soc Jpn* 1992;**100**(4):448–53.
4. Fu CT, Wu JM, Li AK. Microstructure and mechanical properties of Cr_3C_2 particulate reinforced Al_2O_3 matrix composites. *J Mater Sci* 1994;**29**:2671–7.
5. Nakahira A, Niihara K, Ohkijima J, Hirai T. Al_2O_3/Si_3N_4 nano-composites. *J Jpn Soc Powder Powder Metall* 1989;**36**:239–42.
6. Fu C-T, Li A-K. The dependence of surface damage induced by electrical-discharge machining on the fracture strength of Al_2O_3–Cr_3C_2 composites. *Mater Chem Phys* 1994;**39**(2):129–35.
7. Anacleto N, Ostrovski O. Solid-state reduction of chromium oxide by methane-containing gas. *Metal Mater Trans B* 2004;**35B**:609–15.
8. Inoue A, Masumoto T. Formation of nonequilibrium Cr_3C carbide in CrC binary alloys quenched rapidly from the melt. *Scripta Metall* 1979;**13**:711–5.
9. Bewilogua K, Heinitz HJ, Rau B, Schulze S. A chromium carbide phase with B1 structure in thin films prepared by ion plating. *Thin Solid Films* 1988;**167**:233–44.
10. Bouzy E, Bauer-Grosse E, Gaer GL. NaCl and filled Re_3B-type structures for two metastable chromium carbides. *Philos Mag B* 1983;**68**:619–38.
11. Lerch A, Rousset A. Influence of morphology on textural properties and on the reactivity of chromium oxides obtained by decomposition of oxalate precursors $(NH_4)_3[Cr(C_2O_4)_3]$. *Thermochim Acta* 1994;**232**:233–42.
12. Loubière S, Laurent Ch, Bonino JP, Rousset A. Elaboration, microstructure and reactivity of Cr_3C_2 powders of different morphology. *Mater Res Bull* 1995;**30**:1535–46.
13. Loubière S, Laurent Ch, Bonino JP, Rousset A. A metastable chromium carbide powder obtained by carburization of a metastable chromium oxide. *J Alloys Compd* 1996;**243**:59–66.
14. Lozzi L, Passacantando IM, Picozzi P, Santucci S, Crescenzi MD. Electronic structure of Cr clusters on graphite. *Atom Mol Cluster* 1991;**20**:387–90.
15. Fan X, Dickey EC, Pennycook SJ, Sunkara MK. Z-contrast imaging and electron energy-loss spectroscopy analysis of chromium-doped diamond-like carbon films. *Appl Phys Lett* 1999;**75**:2740–2.
16. Buijnsters JG, Shankar P, Fleischer W, Van Enckevort WJP, Schermer JJ, Ter Meulen JJ. CVD diamond deposition on steel using arc-plated chromium nitride interlayer. *Diam Rel Mater* 2002;**11**:536–44.
17. Dresselhaus MS, Dresselhaus G, Sugihara K, Spain IL, Goldberg HA. In: Cardona M, editor. *Graphite fibers and filaments*. Berlin: Springer-Verlag; 1988.
18. Endo M, Koyama T, Hishiyama Y. Structural improvement of carbon fibers prepared from benzene. *Jpn J Appl Phys* 1976;**15**:2073–6.
19. Barshilia HC, Selvakumar N, Rajam KS, Biswas A. Structure and optical properties of pulsed sputter deposited Cr_xO_y/Cr/Cr_2O_3 solar selective coating. *J Appl Phys* 2008;**103**:023507 (1–11).
20. Lin H-T, Wang S-C, Huang J-L, Chang S-Y. Processing of hot pressed Al_2O_3–Cr_2O_3/Cr-carbide nanocomposite prepared by MOCVD in fluidized bed. *J Eur Ceram Soc* 2007;**27**:4759–65.
21. Wang S-C, Chin Y-L, Huang J-L. Microstructure and mechanical properties of hot-pressing chromium carbide/alumina nanocomposite prepared by MOCVD in fluidized bed. *J Eur Ceram Soc* 2008;**28**:1909–16.
22. Lin H-T, Huang J-L, Lo W-T, Wei W-CJ. Investigation on carbonizing behaviors of nanometer-sized Cr_2O_3 particles dispersed on alumina particles by metalorganic chemical vapor deposition in fluidized bed. *J Mater Res* 2005;**20**:2154–60.
23. Arévalo-López AM, Alario-Franco MA. Reliable method for determining the oxidation state in chromium oxides. *Inorg Chem* 2009;**48**:11843–6.

24. Daulton TL, Little BJ, Lowe K, Jones-Meehan J. Electron energy loss spectroscopy techniques for the study of microbial chromium(VI) reduction. *J Microbiol Method* 2002;**50**:39–54.
25. Lacerda RG, Hammer P, Freire Jr FL, Alvarez F, Marques FC. On the structure of argon assisted amorphous carbon films. *Diam Rel Mater* 2000;**9**:796–800.
26. Muradov NZ. CO_2-free production of hydrogen by catalytic pyrolysis of hydrocarbon fuel. *Energy Fuels* 1998;**12**:41–8.
27. Muradov NZ. Hydrogen via methane decomposition: an application for decarbonization of fossil fuels. *Int J Hydrogen Energy* 2001;**26**:1165–75.